Objectives

The overall objective of this work is to identify and understand, via directed experimentation and analysis, the mechanisms which control the structural behavior of fuselages in their response to damage (resistance, tolerance, and arrest). A further objective is to develop straightforward design methodologies which can be employed by structural designers in preliminary design stages to make intelligent choices concerning the material, layup, and structural configuration so that a more efficient structure with structural integrity can be designed and built.

General Approach

Although there are three different facets of the damage issue and these facets do interact, it is possible to first pursue these independently: damage resistance, damage tolerance, and damage arrest. This multiple year effort began with careful consideration of work available in the open literature on damage in general composite structures (e.g. References [1] and [2]) and damage specifically in fuselage-type structures made of composites (e.g. Reference [3]).

The initial work focused on damage growth and damage arrest. It has been shown [4] that the direction of damage propagation can be changed by the particular structural configuration of a pressurized composite cylinder. This indicates that a mechanism does exist by which the path of damage can be altered in composite construction. The next step is to fully arrest the damage. Before proceeding to this next step, the previously tested configurations [4] were structurally analyzed to determine the differences between them. Particular attention was paid to the stiffness and stress field as a function of the propagating damage in an attempt to identify the mechanism(s) which redirect propagating damage.

2

Once these mechanisms were identified, graphite/epoxy cylinders of various structural configurations were designed which isolated the identified mechanisms and thus allowed further testing of the mechanisms.

From this work and the experimental and analytical results, rules of thumb for design will be formulated and further tested in experiment.

Work commenced in Year 2 to study the damage resistance and damage tolerance facets of the damage issue again looking at the same factors as previously mentioned utilizing similar experimental techniques. Damage was initially introduced as through-cracks, but other types of damage will be considered including delamination and other damage combinations which typically occur due to impact of other events. It is recognized that through-cracks do not represent realistic damage to composite structures in service. However, a through-crack is a well-defined damage state and will be used in the initial work to determine the important operative mechanisms in damage arrest. Once the mechanisms have been identified, the more realistic damage states will be considered.

In all cases through this ongoing multi-year effort, analysis will be used to guide the experimentation to isolate specific mechanisms and determine their effects on the damage issues. Initial analysis will continue to be accomplished using the finite element method and appropriate elements. The microcomputer based finite element program COSMOS/M [5] as well as the mainframe programs ADINA [6] and STAGSC-1 [7] will be employed.

Once the mechanisms and parameters are identified, their effects as they are changed will be ascertained so as to determine design methodologies for composite fuselages. Of particular importance are scaling and structural tailoring. Whereas the finite element method is useful in the identification of mechanisms and in point design, emphasis will also be placed on developing more time-efficient analyses suitable for preliminary design stages. These analyses will incorporate the physics of the problem determined through the earlier experimentation and analysis. It is intended that the analyses will thus give the designer a "feel" for the problem as well as allowing the designer to run a number

of parametric studies so that the most effective design can be achieved. Without knowledge of the specific mechanisms involved, it is premature to comment on the exact form these analyses might take.

Year 1 Objectives

During the first year, the work concentrated on identifying the mechanisms by which damage paths can be altered and propagating damage arrested in pressurized composite cylinders. Once these mechanisms were identified, the effects of various configurations on this were to be investigated. This work was anticipated to continue, and did continue, into the second year.

The specific work pursued during the first year to achieve these objectives was as follows. One, the stress/strain field as a function of propagating damage in pressurized fuselages was determined. Two, possible mechanisms and factors in the ability to change the direction of propagating damage were identified. Three, graphite/epoxy plates and cylinders were utilized to examine the mechanisms identified.

Summary of Year 1 Accomplishments

One possible mechanism identified as affecting the direction of propagation of damage was the local change in bending stiffness due to a stiffener placed ahead of the damage. Quasi-isotropic stiffened plates and cylinders using graphite/epoxy fabric with through-thickness slits perpendicular to the primary load direction were fabricated and tested to better understand this mechanism. Analytical work including finite element analysis was performed for both flat plate and cylinder specimens to identify possible mechanisms and

factors related to damage propagation. The specimens were modeled using ADINA [6], a displacement-based finite element code.

Preliminary results for these quasi-isotropic fabric laminates indicate that damage propagates perpendicular to a principal strain direction. In the case of the panels, the stiffeners did not redirect and arrest the damage and the analysis indicated that both the magnitude and orientation of the maximum strain correlate well with the experiment. In the case of the stiffened cylinders, damage bifurcated as the slit grew and redirected along the stiffener. This also correlated well with the analytical results. The conclusion reached is that the local strain field region ahead of the flaw is the controlling factor in subsequent damage propagation and thus in order to control the damage path, the proper structural configuration must be provided. Furthermore, the membrane as well as bending stiffness in this region must be accounted for in any structural analysis used to predict failure. This work is summarized in Reference [8].

Year 2 Objectives

During the second year, the work centered on furthering the investigation of the mechanisms and factors identified in Year 1 with regards to damage propagation and damage arrest as the structural configuration was altered.

The specific work pursued during the second year to achieve these objectives was as follows: One, an experimental program to extend the testing to include the influence of radius of curvature and stacking sequence in the base laminate as well as stiffener configuration and material form on damage tolerance, propagation and arrest was begun. Two, the analysis begun in Year 1 to better understand the damage propagation phenomena observed in both the plates and cylinders was continued.

Also during the second year, the work accomplished in year 1 was fully documented in a master's thesis by Adam Sawicki [9] titled "Damage Tolerance of Integrally Stiffened Composite Plates and Cylinders". An ASTM conference paper [10] and subsequent ASTM STP article were also completed fully documenting the experimental and analytical work conducted on the plate specimens. An abstract detailing the cylinder work was completed and is awaiting submission.

Summary of Work Completed in Year 2

Overview

The notch sensitivity data from Sawicki's plates were analyzed using the Mar-Lin correlation. The results are shown in Figure 1. This correlation can be written as $\sigma_{plate} = H_c (2a)^{-m}$ where σ_{plate} is the far-field failure stress, H_c is the composite fracture parameter, m is the value of notch singularity at the bimaterial interface taken to be equal to 0.28 for graphite/epoxy, and 2a is the flaw length perpendicular to the maximum tensile stress. In addition, Ranniger [11] completed tests using standard TELAC coupons to determine the basic ply properties and notch sensitivity of the solvated resin fabric material AW370/3501-6S. Ranniger [12] also completed notch sensitivity tests using the tape laminate coupons of the same laminate configuration as that used in the 152mm radius tape cylinders. Unstiffened pressurized cylinder tests were performed using 76mm radius fabric cylinders to determine the ability of the Graves' correlation to properly account for (i.e. scale) the cylinder radius and both stiffened and unstiffened tests were performed using 152mm radius tape cylinders to consider the effect of the tape configuration as well as structural anisotropy on the damage tolerance and damage arrest aspects. The Graves' correlation [4] for failure of finite radius cylindrical shells, which modifies the Mar-Lin correlation to account

for the local stress intensification due to the curvature, was used to analyze the cylinder data. This correlation is illustrated in Figure 2.

Experimental Work

Tensile Coupon Tests

Prediction of cylinder failure pressures requires a knowledge of material and laminate properties. The AW370-5H/3501-6S, a five-harness weave impregnated with a solvated resin, had not previously been used in TELAC. Tensile coupon tests were used to determine basic material properties.

Tests were conducted on $[0_f]_4$, $[90_f]_4$, and $[\pm45_f]_S$ tensile coupons to determine the longitudinal, transverse, and shear moduli and the Poisson's ratios of the material system. These results are summarized in Table 1. Tests were conducted on $[0_f/45_f]_S$ tensile coupons with different notch sizes to determine the fracture parameter H_c and to establish a Mar-Lin failure stress correlation. These results are shown in Table 2. The average value for H_C was determined to be $749 MPa*mm^{0.28}$. A schematic of the coupon is shown in Figure 3. Unflawed specimens and those with 6.35 and 9.50mm slits were 355mm long and 50mm wide. Specimens with 19.1 and 12.7 mm slits were 70 mm wide to avoid finite width effects on coupon failure. Slits were oriented perpendicular to the loading axes and were centered on the specimens. Note that the 0° angle designation is aligned with the loading axis in a right-handed coordinate system.

Tensile coupon tests were also conducted on notched and unnotched $[90/0/\pm45]_S$, $[\pm45/90]_S$, and $[\pm45/0]_S$ AS4/3501-6 coupons to obtain values for the composite fracture parameter, H_C, for use in the Mar-Lin failure stress correlation. These results are summarized in Table 3. A schematic of the coupon is shown in Figure 3.

Cylinder Specimens

An experimental program was begun extending the testing to include the influence of radius of curvature and stacking sequence in the base laminate as well as stiffener configuration and material form on damage propagation [11-12]. The first tests were conducted on unstiffened 76mm radius $(0_f/45_f)_s$ laminates to compare directly with Sawicki's 152mm radius cylinder results. The cylinder configuration is illustrated in Figure 4. The endcap system developed for these tests was similar to the previous design and is illustrated in Figure 5. A comparison of the test results for the two cylinder radii and the Graves' failure correlation is shown in Figure 6. Ranniger tested one 152mm radius cylinder with a slit length equal to 12.7mm to further define the damage tolerance of these quasi-isotropic fabric cylinders. As can be seen, the predictive capability is quite good for these quasi-isotropic fabric cylinders indicating that radius of curvature is properly accounted for in the failure prediction. A list of the data for the 76mm radius cylinders is given in Table 4. Failure mode for these 76mm radius unstiffened cylinders is illustrated in Figure 7. This is consistent with the failure mode exhibited by the 152mm radius cylinders tested by Sawicki [9] in which the damage bifurcated and spiraled toward the end of the cylinder. Failure pressure for the 12.7mm slit 152mm radius cylinder was 2.82MPa. Its failure mode was quite different compared to the other quasi-isotropic fabric cylinders and is illustrated in Figure 8. As can be seen there is no clearly definable bifurcation and the damage does not spiral.

To gain a more complete understanding of the influence of stacking sequence, material form, and geometry on the failure of pressurized cylinders, several tape laminates were tested. These included both unstiffened and circumferentially stiffened configurations. In all cases the stiffeners were stacked up on the outside of the cylinder creating an unsymmetric layup. In particular tape quasi-isotropic tape laminates, $[\pm45/0/90]_s$, were tested to compare with the $(0,45)_s$ fabric laminates, and $[\pm45/0]_s$ and $[\pm45/90]_s$ were tested to determine the effects of structural anisotropy on the failure of 152mm radius

cylinders. The failure data for these cylinders is presented in Table 5. Examples of the damage propagation paths are sketched in Figures 9 through 14. Plots of the data comparing the Mar-Lin plate response and Graves' prediction for both isotopic and specially orthotropic [13] are presented in Figures 15 to 17. In all cases for cylinders without stiffening strips, the failure mode is catastrophic and results in a multitude of damage propagation paths. This is in contrast to the results for the fabric cylinders in that for slit sizes greater than 12.7mm the damage propagates from the slits, bifurcates and extends to the ends in a more controlled manner. However, for all cylinders the introduction of the stiffening strips creates damage propagation which is less random and essentially confined to the region defined by the stiffeners. The degree to which this containment occurs depends upon the slit size and the number of stiffening strips. A discussion of this damage arrest and containment is given in the Analysis section below. The damage tolerance of these structurally anisotropic cylinders is still not well understood. The Graves' prediction, for example, does not seem to be a good indicator of the damage tolerance of these structurally anisotropic cylinders. In all cases, the data falls above the prediction and for the 12.7mm slits above the Mar-Lin curve for the flat plate. The quasi-isotropic tape laminate does, however, show good correlation, again except for the 12.7mm slit.

In summary, base laminates using tape ($[\pm45/0]_S$ and $[\pm45/90]_S$) have shown that the predictive capabilities established for the fabric cylinders must be modified to account for the failure modes and additional orthotropy of tape laminates. The $(0,45)_S$ quasi-isotropic fabric laminates, for example, have been shown to be special cases of a more general cylinder failure model.

Analysis

Analysis has continued with an emphasis on understanding the mechanisms responsible for the damage tolerance behavior of the structurally anisotropic cylinders and

9

the damage propagation and containment characteristics of the stiffened cylinders. A preliminary step was taken to identify the critical parameters responsible for damage arrest and containment.

Two observations were used to define a damage containment parameter for these pressurized cylinders. First, comparing the failure modes and damage propagation paths of any one of the laminates reveals a dependence on slit length. It is evident, for example, that severity of damage decreases with slit size for all cylinders. Regardless of the number of stiffeners, the fractures of the specimens with the smallest slit sizes are most severe. Second, in all cases investigated to date, the presence of stiffeners drastically affected the direction of damage propagation after initial fracture. These circumferential stiffening bands were shown analytically for the fabric cylinders to lower the magnitude and shift the direction of the principal strains ahead of the slit [9]. The thickness of the stiffening layer which affects the bending stiffness will then directly affect these local strain fields. The quantitative method proposed by Ranniger [12] of evaluating stiffener effectiveness in containing or turning damage paths therefore included both measures of slit size or failure pressure and of bending stiffness. A laminate-specific containment ratio, C, dependent upon these measures was proposed:

$$C = \frac{D_s}{D_u}\left(\frac{2a}{R}\right)$$

This non-dimensional containment factor is dependent upon the ratio of the circumferential bending stiffness of the stiffened regions, D_s, to that of the unstiffened base laminate, D_u. The slit length, 2a, is non-dimensionalized by the cylinder radius, R, thus incorporating the effects of specimen curvature. The value of the containment ratio increases with likelihood of turning or containing damage originating at a slit end between the set of stiffeners. As the radius of a cylinder approaches infinity and the specimen approximates a flat plate, the value of the containment ratio approaches zero. Work by Sawicki [10], which

10

shows that stiffeners have no effect on the direction of notch propagation in comparable flat plates, supports the use of the radius, R, in the denominator of the containment ratio.

Values of the containment ratios were compared with qualitative estimations of the state of cylinder damage and effectiveness of stiffeners in redirecting fracture paths in the circumferential direction. For the purposes of this investigation, the damage of the cylinders was described in terms of three words: 'through', 'turned', or 'into'. These words correspond to the extent of the fracture paths relative to the stiffener locations. 'Through' indicates that at least one fracture path extended entirely through the stiffening band, or in the case of unstiffened cylinders, all the way to the endcaps. 'Into' indicates that a fracture path traveled at least partway into the stiffened region, and 'turned' indicates that the fracture path was turned to 0° at the inside edge or within the width the stiffener. More than one term may apply to each cylinder. However, a direct comparison of containment ratio values and schematics of the individual stiffener damage states may be more enlightening.

Values of the containment ratios for the individual cylinders are presented with the qualitative descriptions in Tables 6 and 7. With the exception of the [±45/0]$_S$ cylinder with two stiffeners and a 63.5 mm slit, the qualitative and quantitative measures of cylinder damage correlate within each laminate type. It is important to note that the correlations are laminate specific. The applicability of this containment ratio to other cylinder types is untested.

Preliminary Results

The following are preliminary conclusions reached concerning the tests on 76mm radius fabric cylinders and 152mm radius tape cylinders. The Graves' prediction for damage tolerance of pressurized cylinders can be used to predict the failure of 76mm as well as 152mm radius quasi-isotropic fabric and tape graphite/epoxy cylinders with axial

slits. Except for the case of the 12.7mm slit in the quasi-isotropic tape cylinder, the data correlates well with this predictive method. An explanation for this behavior should be pursued analytically and experimentally. Damage tolerance of the structurally anisotropic [±45/0]s and [±45/90]s tape cylinders with slit sizes ranging from 12.7 to 63.5mm are not predictable using the Graves' method as currently interpreted. Laminate properties such as structural coupling as well as the biaxial loading state, not included in the predictive method, may be important factors. External stiffening bands located on either side of a slit generally redirect fracture paths from the axial to the circumferential direction. The amount of redirection depends on the number of stiffeners as well as the internal pressure applied to the cylinder. Ability of the stiffening bands to contain damage depends both on the slit size and the number of stiffener layers present in the cylinder. Quantification of this effect has been attempted via a containment ratio dependent on slit length, cylinder radius, and the bending stiffnesses of the stiffened and unstiffened regions. The containment ratio successfully ranks the structurally anisotropic cylinders according to the amount of damage extending through the stiffeners.

A Master's thesis fully documenting much of the effort in Year 2 is being completed.

Plans for Year 3

Initially during the third year, the work accomplished in Year 2 will be fully documented in a Master's thesis. The work will progress to further investigate the mechanisms identified in Years 1 and 2 and extensions of these results as the structural configuration is altered. It is hoped that this will culminate in the identification of structural configurations which will successfully arrest damage and which can be tested in the ensuing years.

The specific work to be pursued during the third year is as follows: (1) Extend the existing damage tolerance prediction methodology to the general case to include the effects of structural orthotropy and diverse failure modes. (2) Continue the analysis and make refinements to include the effects of stacking sequence and gradient stress field ahead of the damage in the cylinder models. Use the analysis to identify and conduct critical experiments defined as those which will test the identified damage arrest mechanisms. (3) Using the developed analysis techniques, plan an experimental program utilizing plates and cylinders to verify the mechanisms identified as efficient damage arrest schemes.

REFERENCES

1. *Advanced Organic Composite Materials for Aircraft Structures - Future Program*, Report of the National Research Council Committee on the Status and Viability of Composite Materials for Aircraft Structures, National Academy Press, Washington, D.C., 1987.

2. "Damage Tolerance of Composites", Final Government/Industry Review of USAF Contract F33615-82-C-3213, presented at Monterey, California, April, 1987.

3. P.A. Lagace and K.J. Saeger, "Damage Tolerance Characteristics of Pressurized Graphite/Epoxy Cylinders", *Proceedings of the Sixth International Symposium on Offshore Mechanics and Arctic Engineering*, ASME, Houston, Texas, March, 1987, pp. 31-37.

4. M.J. Graves and P.A. Lagace, "Damage Tolerance of Composite Cylinders", *Composite Structures*, Vol. 4, No.1, 1985, pp. 75-91.

5. COSMOS/M Release 1.65, Structural Research & Analysis Corporation, 1661 Lincoln Boulevard, Suite 200, Santa Monica, CA, 1992.

6   "Automatic Dynamic Incremental Nonlinear Analysis-Input:User's Manual," Report ARD 87-4, ADINA R. & D., Inc., 1987.

7. STAGSC-1, Structural Analysis of General Shells, NASA.

8. Graves, M.J. and Lagace, P.A., "Composite Fuselage Technology--Annual Report for period April 7, 1989 to April 6, 1990 on NASA Langley Research Grant NAG-1-991", TELAC Report 90-19, October, 1990.

9. A.J. Sawicki, "Damage Tolerance of Integrally Stifffened Composite Plates and Cylinders", TELAC Report 90-17, Massachusetts Institute of Technology, September, 1990.

10. A.J. Sawicki, M.J. Graves, and P.A. Lagace, "Failure of Graphite/Epoxy Panels with Stiffening Strips", ASTM Fourth Symposium on Composite Materials: Fatigue and Fracture, May 6-7, 1991, Indianapolis, Indiana.

11. C.U Ranniger, "Effect of Cylinder Diameter on the Damage Tolerance of Graphite/Epoxy Cylinders with Axial Notches", TELAC Report 91-10, Massachusetts Institute of Technology, May, 1991.

12. C.U. Ranniger, "Damage Tolerance and Arrest Characteristics of Pressurized Graphite/Epoxy Tape Cylinders", TELAC Report 91-11, Massachusetts Institute of Technology, June, 1991.

13. M.J. Graves, "The Catastropic Failure of Pressurized Graphite/Epoxy Cylinders," PhD Thesis, Massachusetts Institute of Technology, September 1982.

Figure 1 Mar-Lin prediction and experimental failure stresses versus slit size for Sawicki's plate specimens

Far-Field Failure Stress versus Slit Length for Panel Specimens
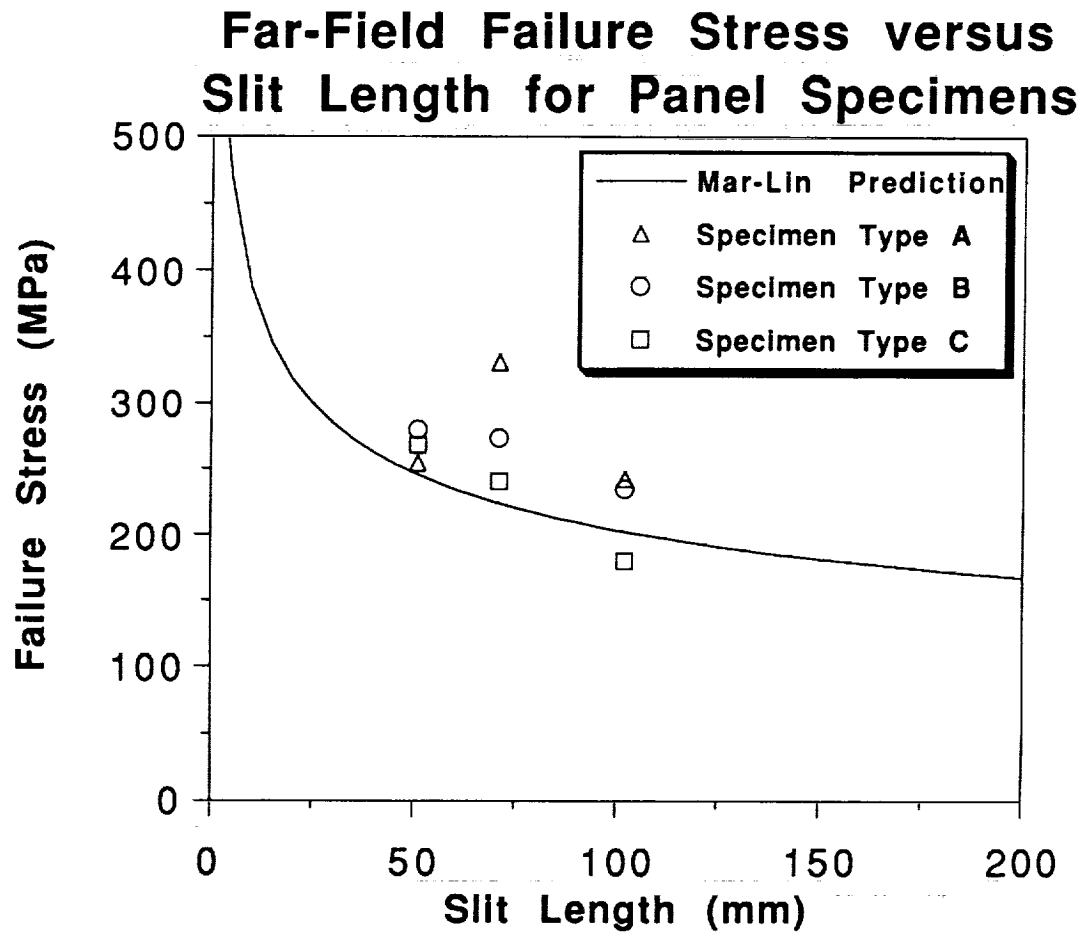
Figure 2 Graves' failure correlation for isotropic cylindrical shells

$$\sigma_{Hoop} = \frac{P\,R}{t}$$

$$\sigma_{Axial} = \frac{P\,R}{2\,t}$$
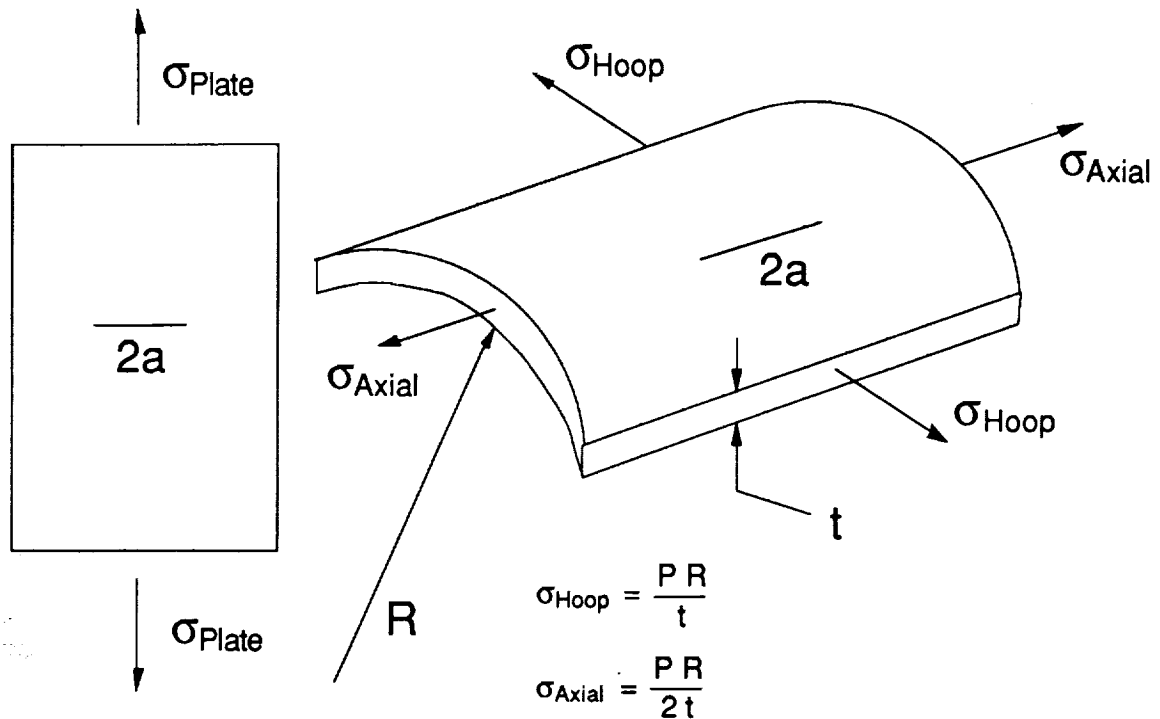
$$\frac{\sigma_{Hoop}}{\sigma_{Plate}} = \frac{1}{[1 + 0.317\,\lambda^2]^{\frac{1}{2}}}$$

Where

$$\lambda^2 = \frac{a^2[12(1 - v^2)]^{\frac{1}{2}}}{R\,t}$$

a = Half Slit Length
v = Poisson's Ratio
R = Radius of Curvature
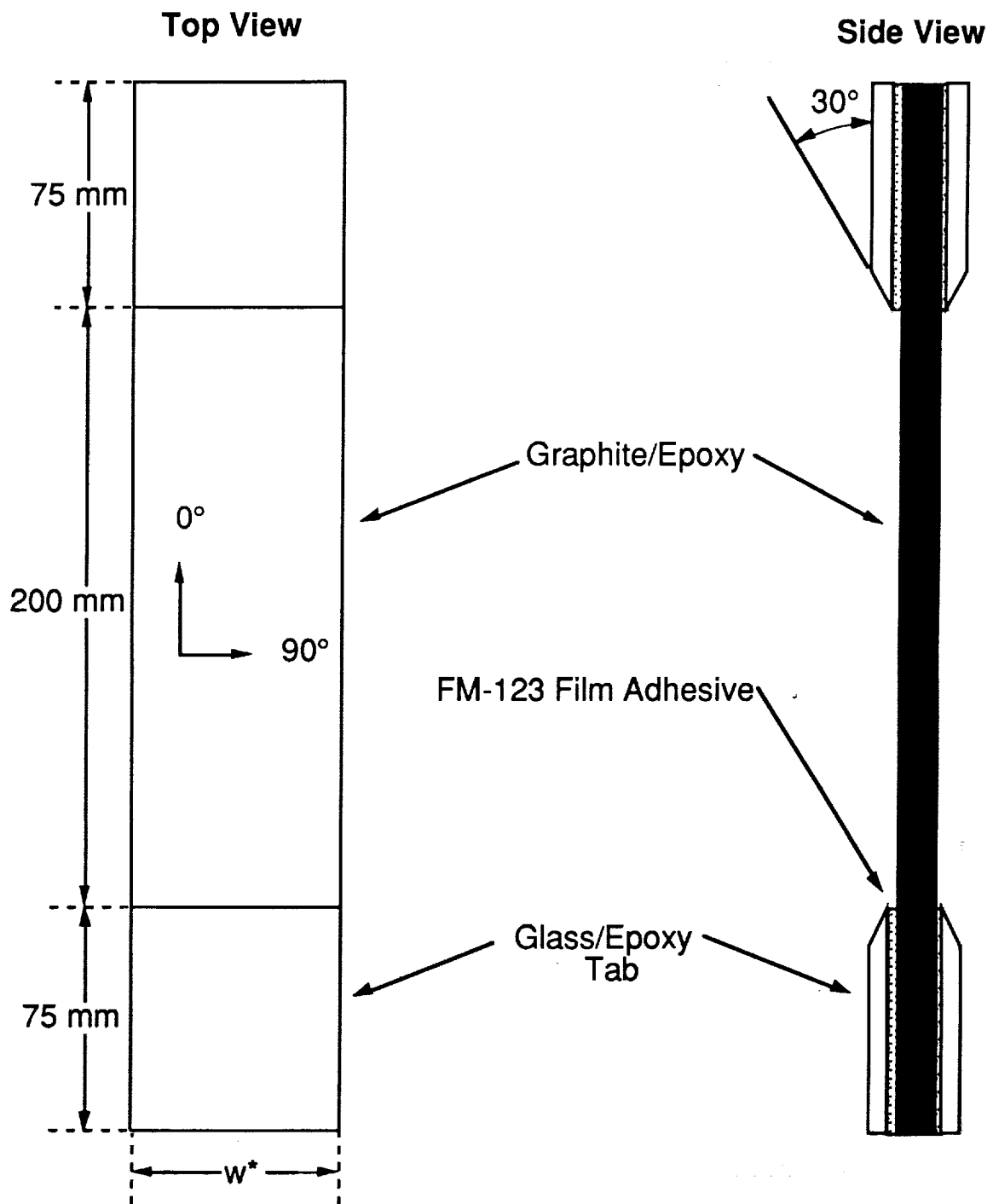t = Thickness
P = Pressure
σ_{Hoop} = Failure Stress of Pressurized Cylinder
σ_{Plate} = Failure Stress of Flat Plate = $H_C\,(2a)^{-m}$

16

Figure 3 Tensile coupon configuration used to determine material properties and notch sensitivity

Top View

Side View

75 mm

200 mm

0°

90°

Graphite/Epoxy

FM-123 Film Adhesive

Glass/Epoxy
Tab

30°

75 mm

w*
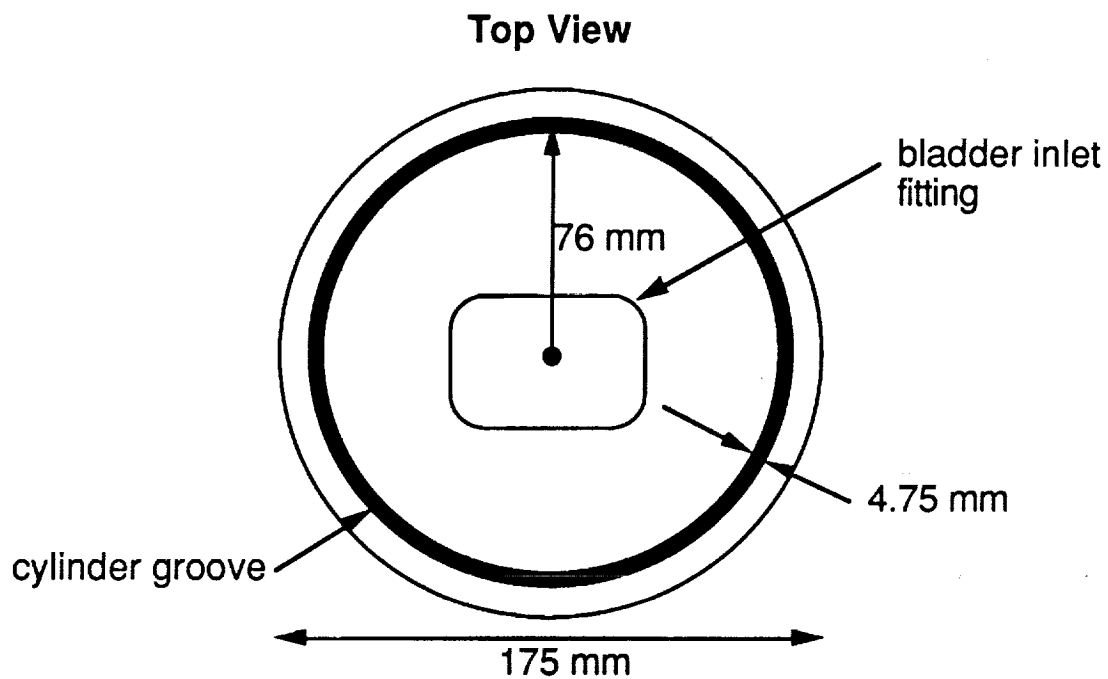
* for unflawed coupons and those with 6.35 and 9.50 mm slits, w = 50 mm
for coupons with 12.7 and 19.1 mm slits, w = 70 mm
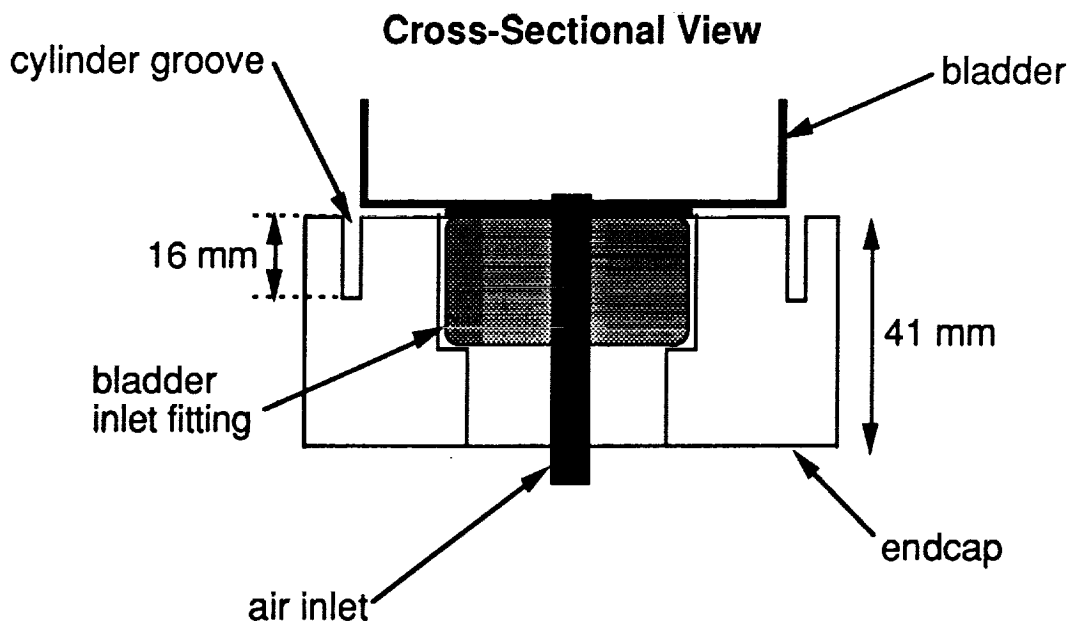
Figure 4 Cylinder configuration
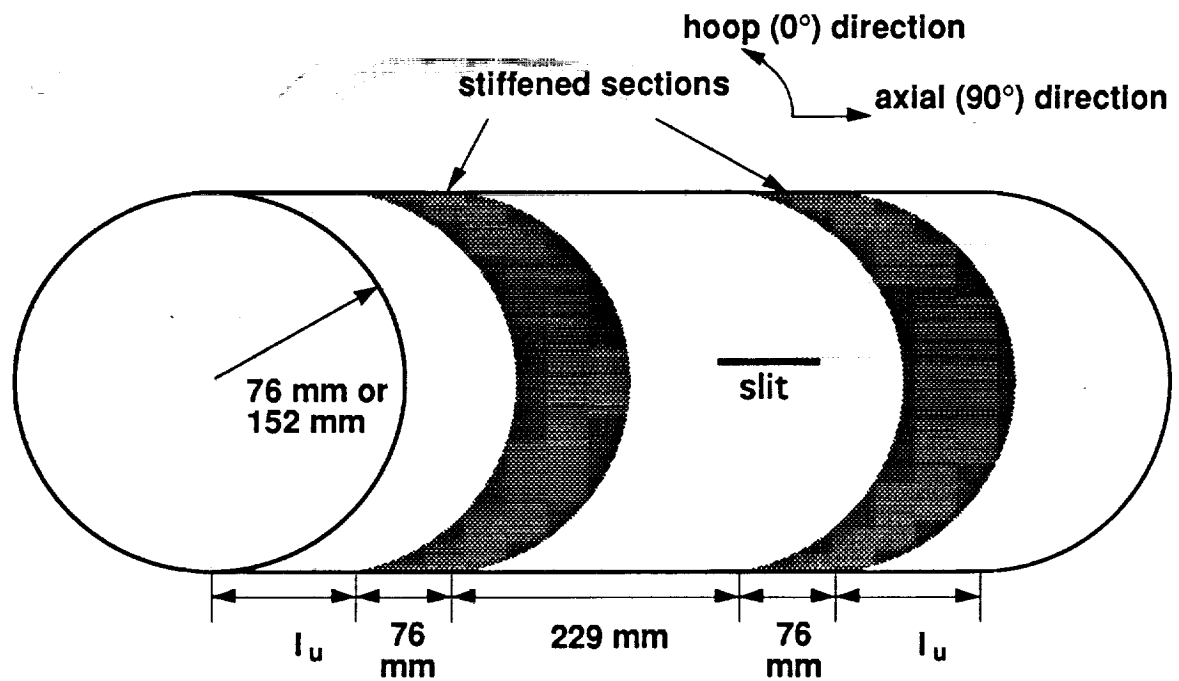
I_u = distance between end of cylinder and stiffener
= minimum of 114 mm

Figure 5 Schematic of endcap and bladder fitting for the 76mm radius cylinder tests

Top View
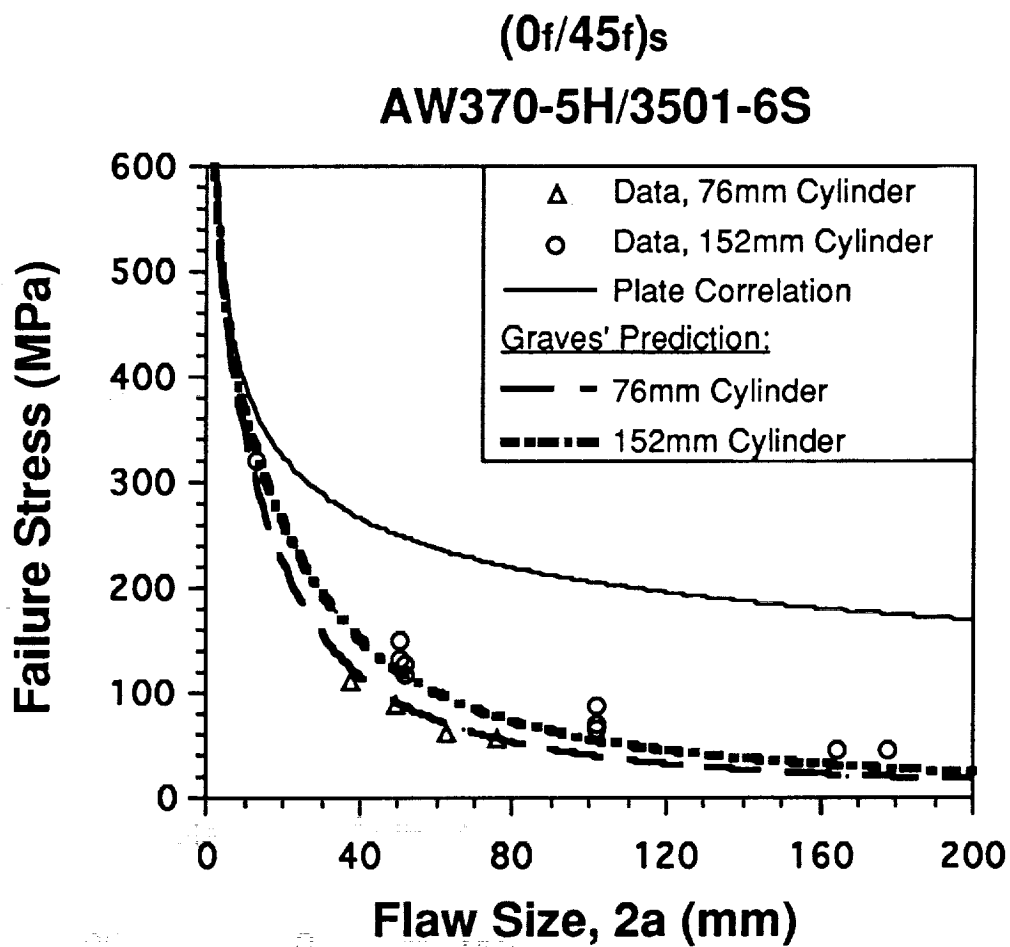
bladder inlet fitting

76 mm

4.75 mm

cylinder groove

175 mm

NOTE: Bladder Fitting is in One of Two Endcaps Only

Cross-Sectional View

cylinder groove

bladder

16 mm

41 mm

bladder inlet fitting

endcap

air inlet

NOTE: Not to Scale

Figure 6 Cylinder data and Graves' failure prediction curve for 76mm 152mm radius (0f/45f)s cylinders

(0f/45f)s

AW370-5H/3501-6S

Legend:
- △ Data, 76mm Cylinder
- ○ Data, 152mm Cylinder
- —— Plate Correlation
- Graves' Prediction:
- — — 76mm Cylinder
- ▬▬▬ 152mm Cylinder

Y-axis: Failure Stress (MPa)

X-axis: Flaw Size, 2a (mm)

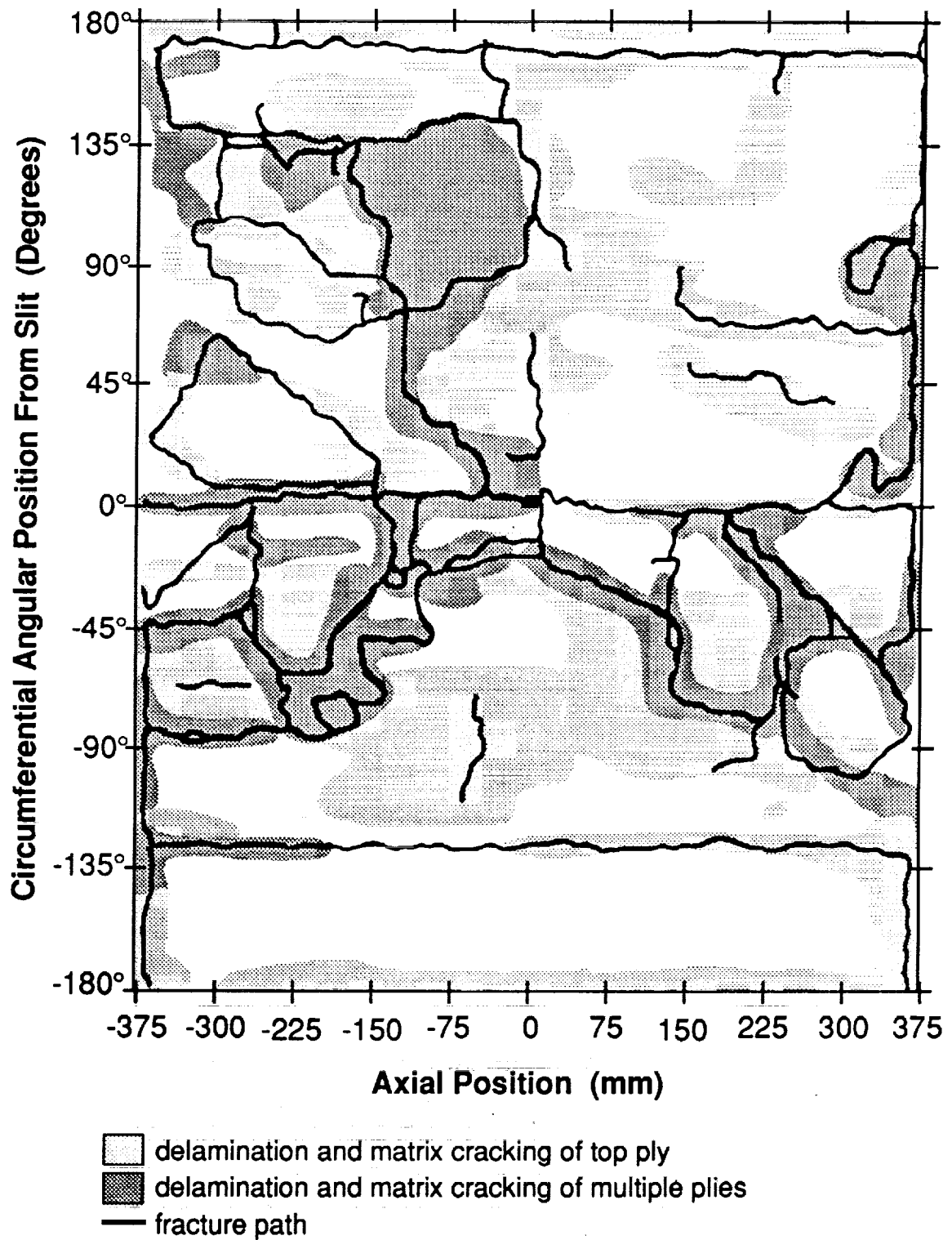**Figure 7**   Sketch of typical damage propagation path for 76mm radius $(0_f/45_f)_S$ cylinder
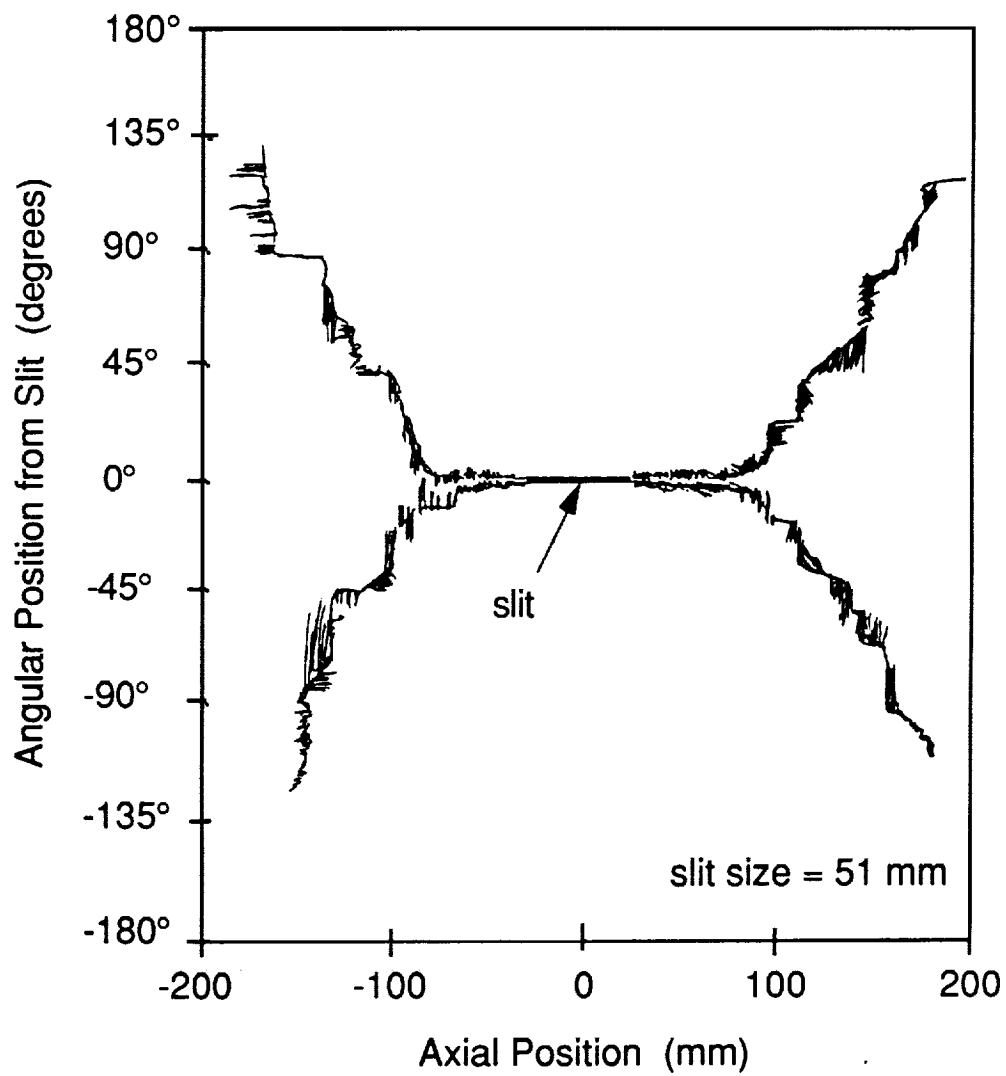
Figure 8 Sketch of damage propagation path for 152mm radius (0f/45f)s cylinder with 12.7mm slit and no stiffeners

Axial Position (mm)

░ delamination
— fracture path
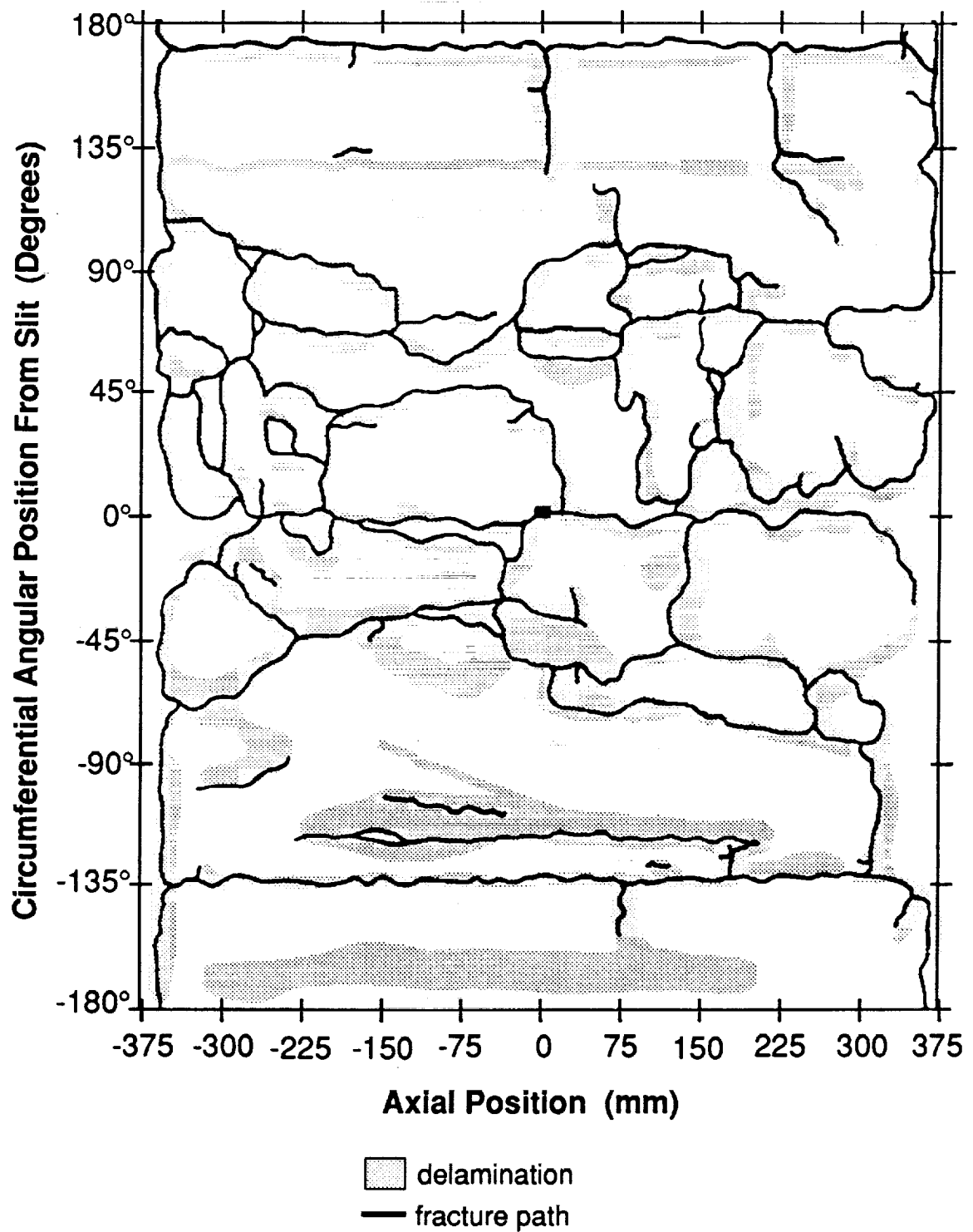
Figure 9   Sketch of damage propagation path for 152mm radius [90/0/±45]s cylinder with 12.7mm slit and no stiffeners

delamination and matrix cracking of top ply
delamination and matrix cracking of multiple plies
— fracture path

Figure 10 Sketch of damage propagation path for 152mm radius [90/0/±45]$_S$ cylinder with 50.8mm slit and no stiffeners

☐ delamination and matrix cracking of top ply
■ delamination and matrix cracking of multiple plies
— fracture path
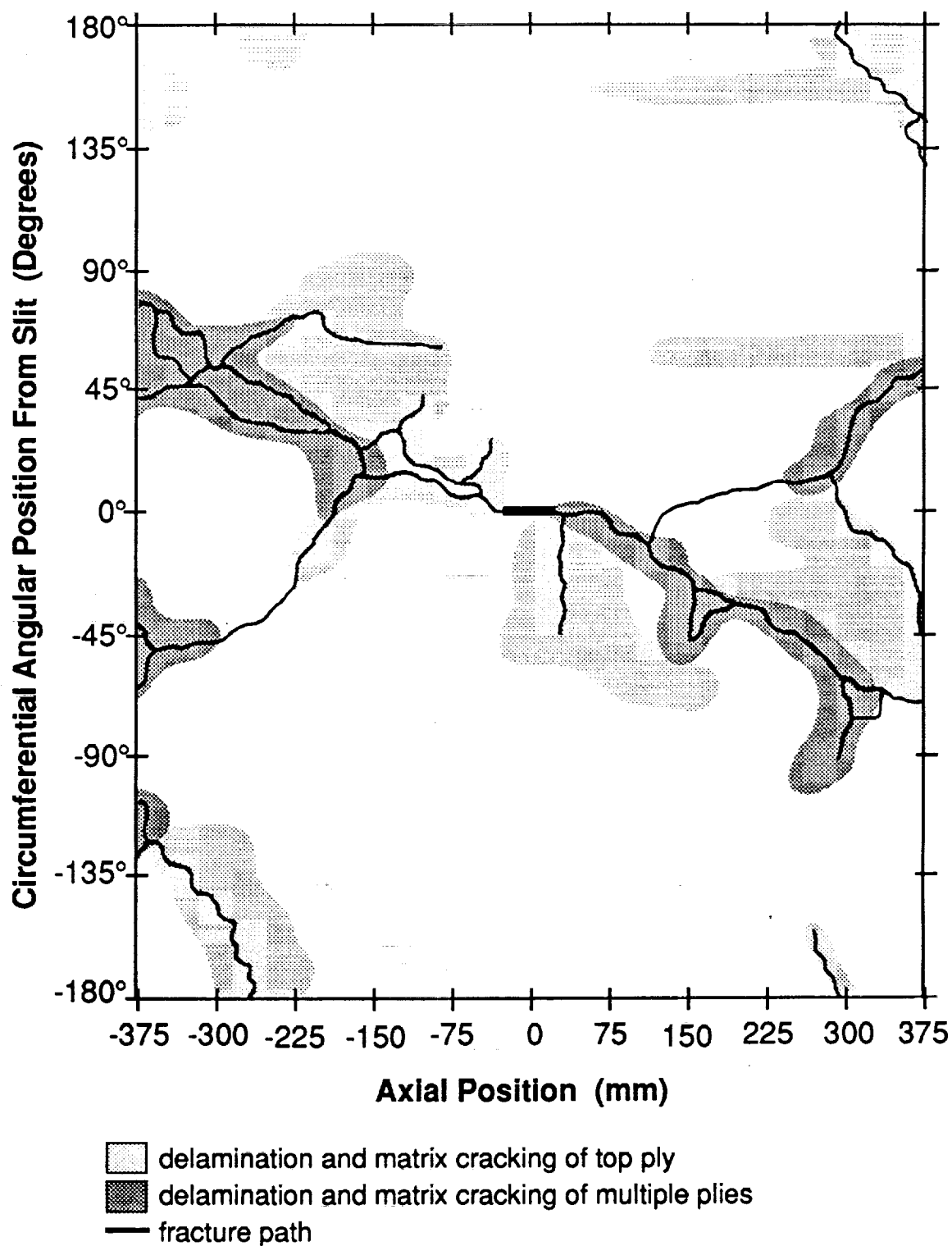
Figure 11 Sketch of damage propagation path for 152mm radius [±45/0]$_S$ cylinder with 25.4mm slit and no stiffeners

- ▢ delamination and matrix cracking of top ply
- ▨ delamination and matrix cracking of multiple plies
- — fracture path

Figure 12 Sketch of damage propagation path for 152mm radius [±45/0]S cylinder with 38.1mm slit and four layers of stiffeners

delamination and matrix cracking of top ply
delamination and matrix cracking of multiple plies
delamination and matrix cracking of stiffener plies
—— fracture path
— — stiffener edges

Figure 13 Sketch of damage propagation path for 152mm radius [±45/90]$_S$ cylinder with 38.1mm slit and no stiffeners
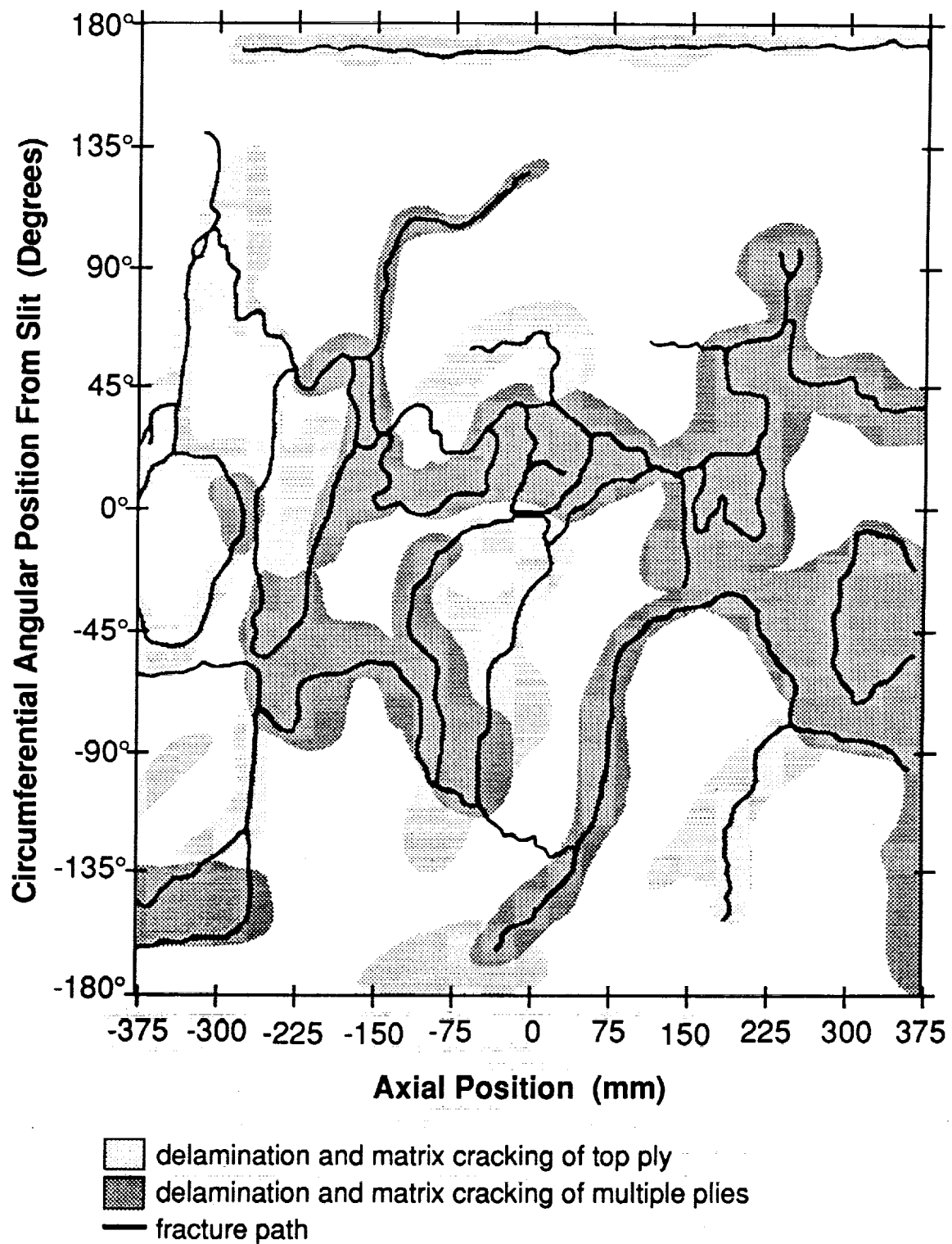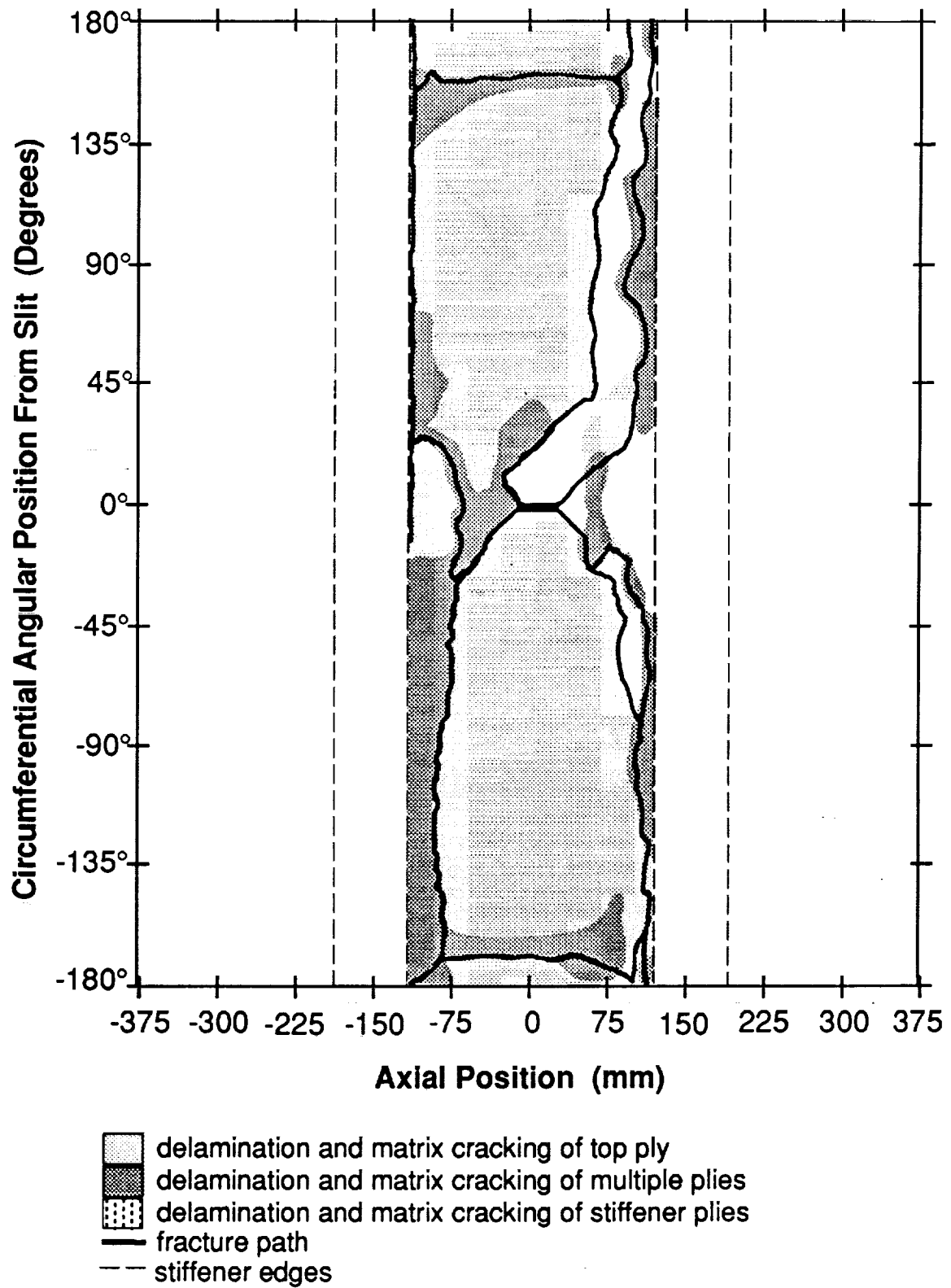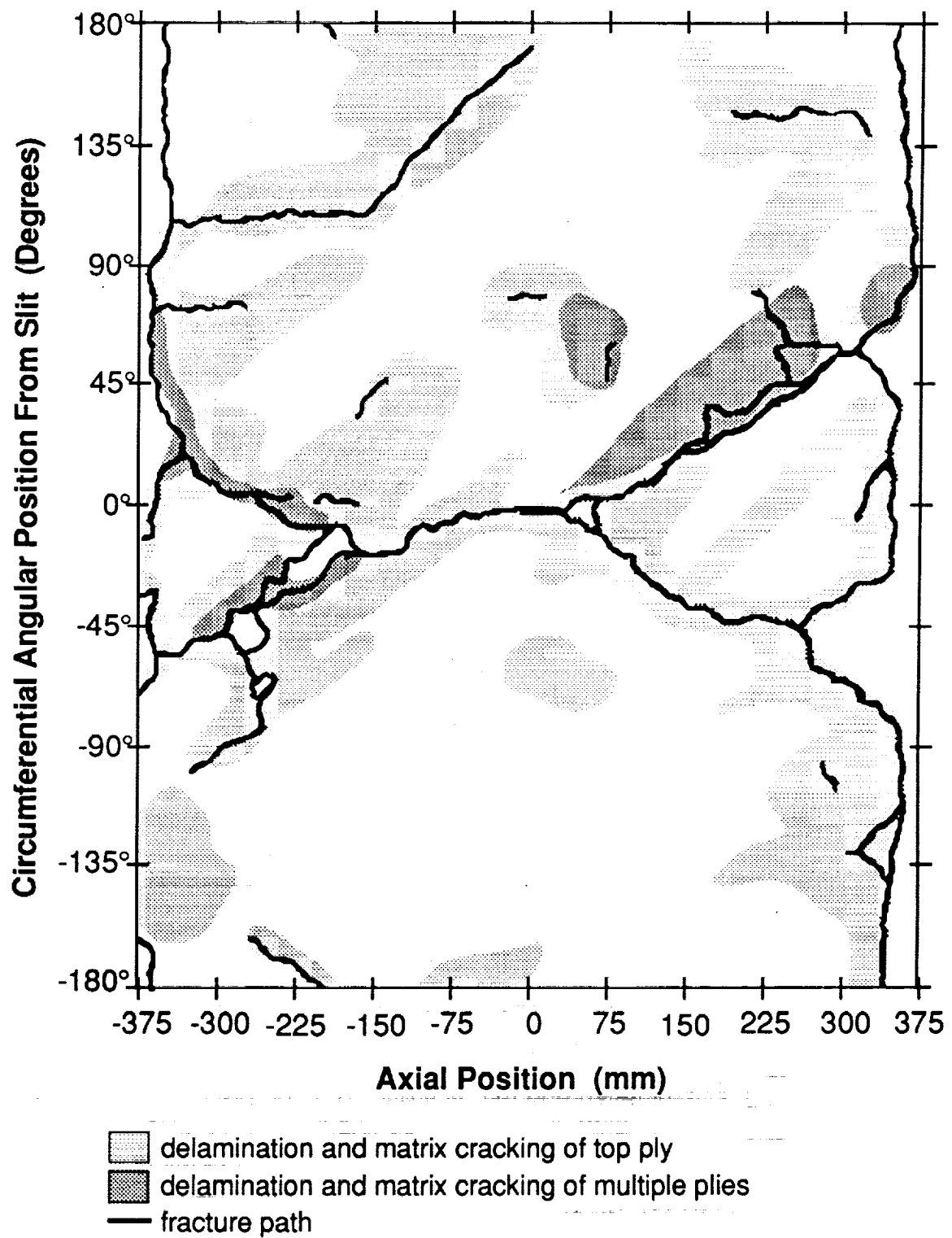

delamination and matrix cracking of top ply
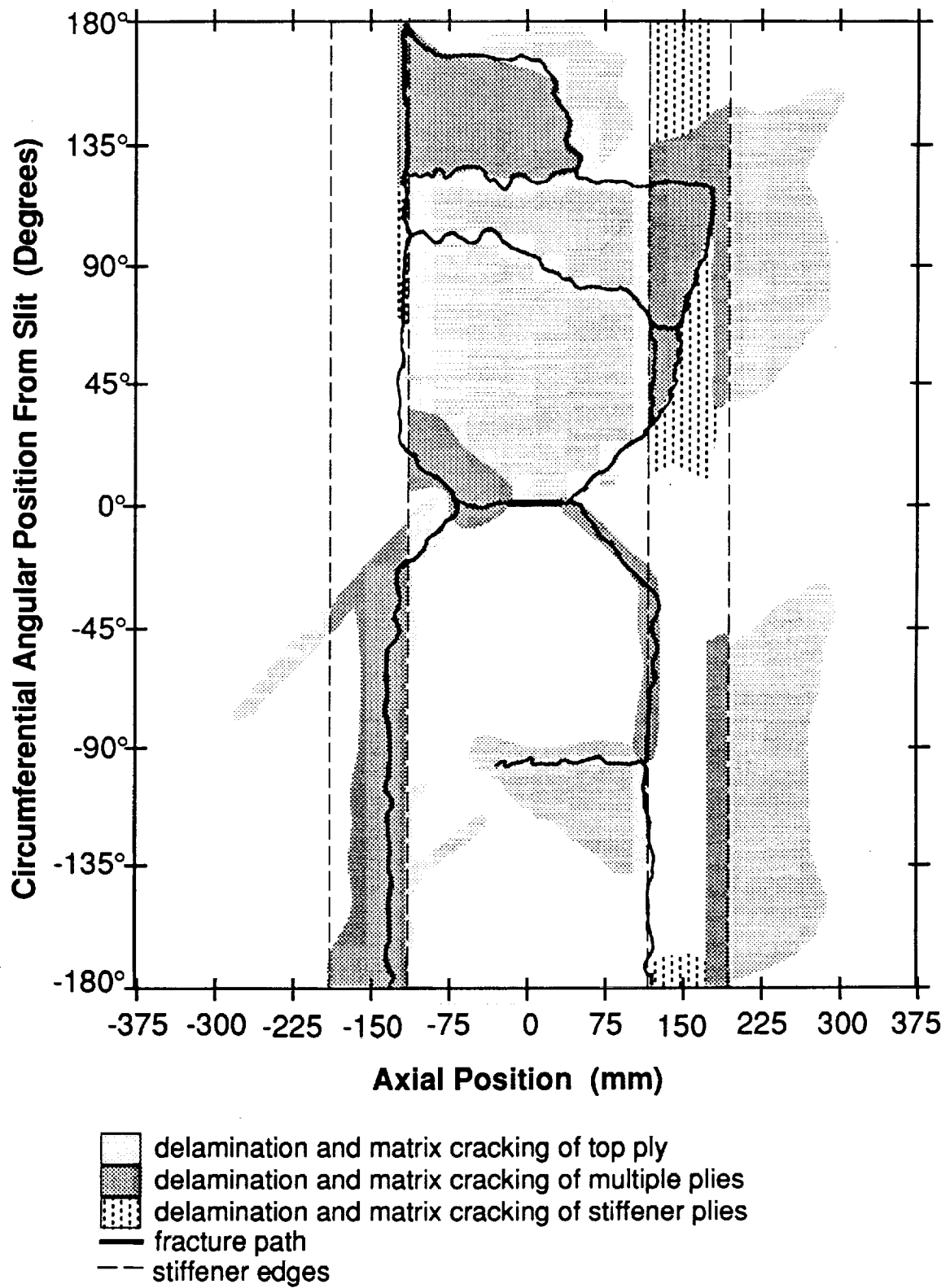delamination and matrix cracking of multiple plies
— fracture path

Figure 14 Sketch of damage propagation path for 152mm radius [±45/90]s cylinder with 50.8mm slit and four layers of stiffeners

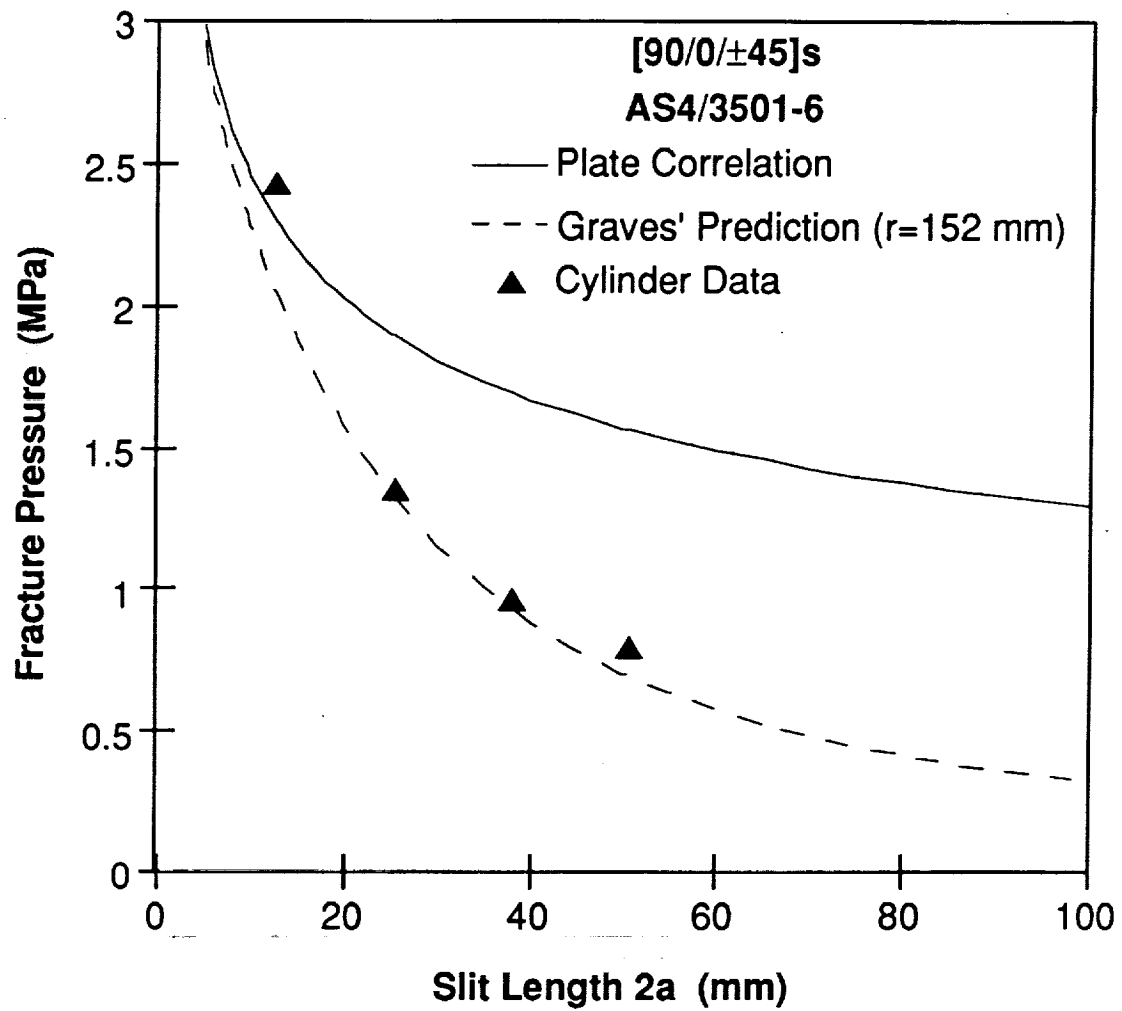delamination and matrix cracking of top ply
delamination and matrix cracking of multiple plies
delamination and matrix cracking of stiffener plies
—— fracture path
— — stiffener edges

Figure 15 [90/0/±45]s 152mm cylinder failure pressure and prediction curves

Figure 16 [±45/0]s 152mm cylinder failure pressure and prediction curves

———— Plate Correlation
– – – Graves' Isotropic Shell Prediction
----- Graves' Orthotropic Shell Prediction
▲ Cylinder Data (r = 152 mm)

[±45/0]s
AS4/3501-6

Y-axis: Fracture Pressure (MPa)
X-axis: Slit Length 2a (mm)
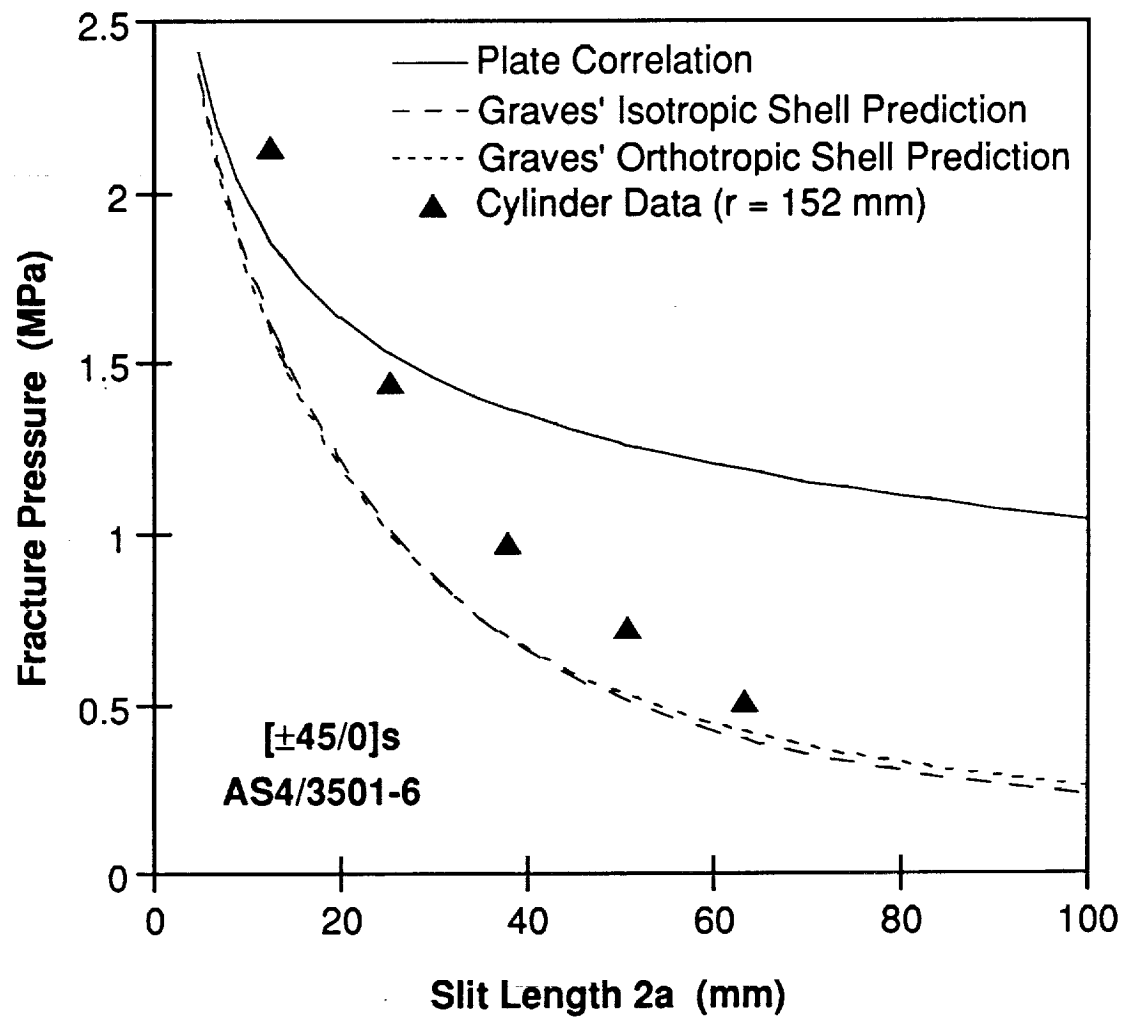
Figure 17 [±45/90]s 152mm cylinder failure pressure and prediction curves
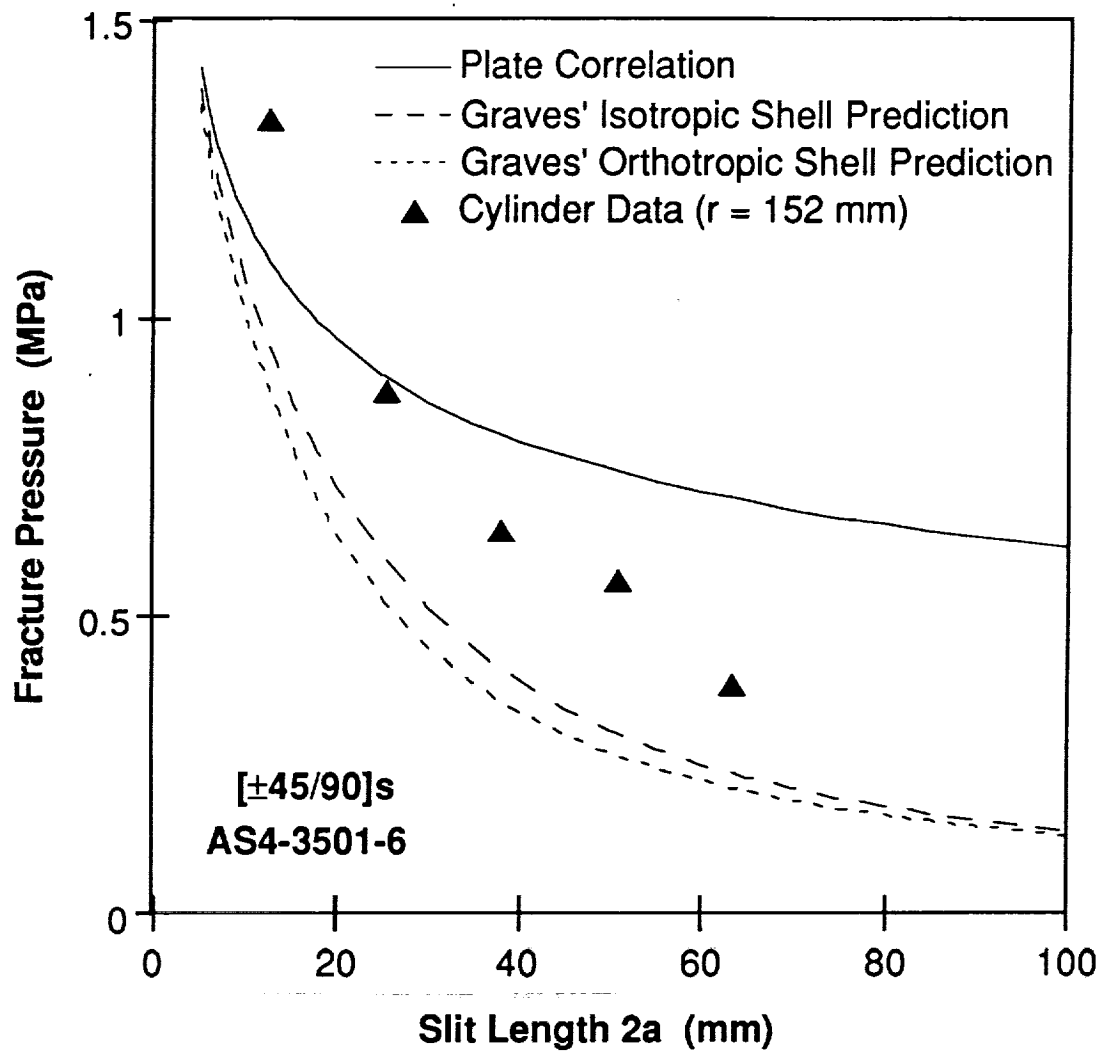
Table 1 Test results used to determine the tensile material properties of AW370-5H/3501-6S

[0f]4		[90f]4		[±45f]s
E_L (GPa)	ν_{LT}	E_T (GPa)	ν_{TL}	G_{LT} (GPa)
72.3	0.066	74.4	0.043	5.97
74.9	0.033	69.0	0.038	6.80
67.7	0.084	71.0	0.073	6.34
78.4	0.102	75.4	0.051	6.32
80.1	----[a]	75.4	0.048	6.84
75.5	0.032			
73.2	0.065			
74.6	0.041			
72.4	0.059			
71.7	0.064			
Average **74.1** (4.7%)[b]	Average **0.061** (38.0%)	Average **73.1** (3.9%)	Average **0.051** (26.4%)	Average **6.45** (5.7%)

[a] data lost due to gage failure

[b] numbers in parentheses are coefficients of variation

Table 2   Test data used to determine H_C for $[0_f/45_f]_s$

Actual Slit Length (mm)	Average Width (mm)	Average Thickness (mm)	Failure Stress (MPa)	H_C (MPa*mm$^{0.28}$)
6.5	49.9	1.27	451	762
6.5	50	1.28	447	755
6.3	49.8	1.3	447	750
6.3	50	1.29	429	718
6.7	49.7	1.32	423	721
9.6	49.7	1.28	397	747
9.3	49.9	1.31	380	708
9.2	49.9	1.32	392	730
9.6	49.8	1.3	397	748
9.3	49.7	1.3	384	718
13.0	70.0	1.3	372	762
12.5	70.0	1.29	372	754
12.6	70.0	1.33	375	763
12.2	70.0	1.3	381	767
18.8	70.6	1.32	332	755
19.0	70.5	1.35	352	803
19.0	70.6	1.34	337	770
18.9	70.6	1.32	330	750
				Average **749** (3.1%)[a]

[a] number in parenthesis is coefficient of variation

33

Table 3 Values for H_c for tape laminates $[90/0/\pm45]_s$, $[\pm45/0]_s$, and $[\pm45/90]_s$

	Nominal Slit Length {Number of coupons} (mm)	Average Fracture Stress (MPa)	Average H_c (MPa*mm$^{0.28}$)
$[90/0/\pm45]_s$	unnotched {3}	621 (10.6%)[a]	--
	9.5 {4}	342 (4.8%)	643 (4.7%)
	12.7 {4}	334 (1.1%)	680 (1.2%)
	15.9 {4}	314 (2.7%)	681 (2.7%)
	19.1 {4}	286 (5.0%)	653 (5.0%)
			Average **664** (4.2%)
$[\pm45/0]_s$	unnotched {8}	743 (13.4%)	--
	9.5 {4}	392 (4.2%)	754 (5.0%)
	12.7 {4}	344 (3.9%)	709 (2.4%)
	15.9 {4}	311 (6.5%)	680 (6.1%)
	19.1 {4}	313 (4.8%)	718 (4.1%)
			Average **715** (5.6%)
$[\pm45/90]_s$	unnotched {8}	224 (3.9%)	--
	9.5 {4}	218 (3.4%)	411 (3.5%)
	12.7 {4}	205 (4.3%)	421 (5.2%)
	15.9 {4}	197 (4.3%)	427 (4.1%)
	19.1 {3}	189 (4.6%)	431 (4.5%)
			Average **422** (4.3%)

[a] numbers in parentheses are coefficients of variation

Table 4   Data for Ranniger's 76mm radius $(0_f/45_f)_s$ cylinders

Slit Length (mm)	Average Thickness (mm)	Failure Pressure (MPa)
38	1.29	1.90
50	1.30	1.51
63	1.33	1.05
76	1.32	0.97

Table 5   Data for Ranniger's 152mm radius tape cylinders

Slit Size (mm)		Number of Stiffener Layers	Failure Pressure (MPa)
[90/0/±45]s	12.7	0	2.42
	25.4	0	1.34
	38.1	0	0.96
	50.8	0	0.79
[±45/0]s	12.7	4	2.13
	25.4	0	1.44
	38.1	4	0.97
	50.8	2	0.72
	63.5	2	0.50
[±45/90]s	12.7	4	1.33
	25.4	0	0.88
	38.1	0	0.64
	50.8	4	0.56
	63.5	2	0.38

Table 6   Qualitative and quantitative fracture assessment of [±45/0]s
cylinders

Slit Size (mm)	Number of Stiffener Layers	Containment Ratio	Qualitative Fracture Description
12.7	4	1.50	through
25.4	0	0.17	through
38.1	4	4.49	turned
50.8	2	2.09	into/turned
63.5	2	2.61	through/turned[a]

[a] fracture extends through the stiffeners but turns before reaching the endcaps

Table 7 Qualitative and quantitative fracture assessment of [±45/90]s cylinders

Slit Size (mm)	Number of Stiffener Layers	Containment Ratio	Qualitative Fracture Description
12.7	4	1.65	through/turned
25.4	0	0.17	through
38.1	0	0.25	through
50.8	4	6.62	into/turned
63.5	2	2.85	through/turned